Enhancing the Science Return of the Spitzer Warm Mission[1]

Kenneth Mighell
National Optical Astronomy Observatory, 950 N. Cherry Ave., Tucson, AZ 85719

ABSTRACT

Planning is underway for the post-cryogenic ("warm") operation of the *Spitzer Space Telescope* which will start around April 2009 after all of the liquid helium has been depleted. Only channels 1 and 2 (3.6 and 4.5 microns) of Spitzer's Infrared Array Camera (IRAC) will be operational at full sensitivity at that time -- providing an unmatched sensitivity from 3 to 5 microns until the *James Webb Space Telescope* is launched. The other channels of all remaining instruments will not operate at the elevated temperatures (25-30K) of Spitzer will experience during its warm mission phase. Last year at AMOS 2006, I showed how the recorded flux of bright point sources observed with IRAC Ch1 is corrupted by lossy detectors which have large intrapixel quantum efficiency variations. During the past year, I have worked closely with members of Spitzer's IRAC Instrument Team to demonstrate that my NASA-funded MATPHOT algorithm for precision stellar photometry and astrometry can yield an improvement in the precision of stellar photometry obtained from IRAC Ch1 observations of bright stars of more than 100% over the best results obtained with aperture photometry corrected with the radial correction recommended in the IRAC Data Handbook. I describe some results of an ongoing effort to develop new calibration procedures for IRAC Ch1 and Ch2 which have the potential of significantly improving the precision of IRAC bright point-source photometry. This timely research effort is intended to not only enhance the science return of existing IRAC Ch1 observations in the Spitzer data archive but also those that will be made during the Spitzer Warm Mission.

1. SPITZER SPACE TELESCOPE'S WARM MISSION

The *Spitzer Space Telescope (SST)* was launched into an Earth-trailing orbit from the Kennedy Space Flight Center on 2003 August 25 UT (see Fig. 1) [1]. The 85-cm cryogenically cooled beryllium Ritchey-Chretien telescope system operates at temperatures as low as 5.5 K. Planning is underway for the post-cryogenic ("warm") operation of the *Spitzer Space Telescope* which will start around April 2009 after all of the liquid helium has been depleted. Only channels 1 and 2 (3.6 and 4.5 microns) of Spitzer's Infrared Array Camera (IRAC; [2]) will be operational at full sensitivity at that time -- providing an unmatched sensitivity from 3 to 5 microns until the *James Webb Space Telescope* is launched. The other channels of all remaining instruments will not operate at the elevated temperatures (25-30K) of Spitzer will experience during its warm mission phase. This article describe some results of an ongoing effort to develop new calibration procedures for IRAC Ch1 and Ch2 which have the potential of significantly improving the precision of IRAC bright point-source photometry. This timely research effort is intended to not only enhance the science return of existing IRAC Ch1 and Ch2 observations in the Spitzer data archive but also those that will be made during the Spitzer Warm Mission.

[1] This work is based on archival data obtained with the *Spitzer Space Telescope*, which is operated by the Jet Propulsion Laboratory, California Institute of Technology under a contract with NASA. Support for this work was provided by an award issued by JPL/Caltech.

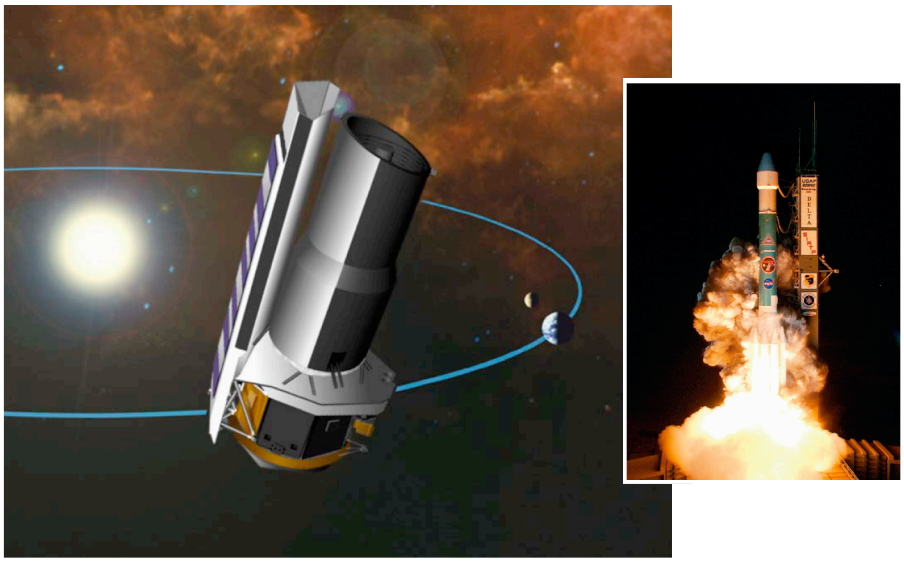

Fig. 1. This artist rendition shows an external view of the *Spitzer Space Telescope* in its Earth-trailing solar orbit. The insert image shows the launch of the *SST* from the Kennedy Space Flight Center on 2003 August 25 UT [1].

2. OBSERVATIONS AND PHOTOMETRIC REDUCTIONS

Sixteen short (0.4 s) calibration observations of the K0 star PPM 9412 were obtained on 2003 October 8 UT with Channel 1 (3.6 μm) of the Infrared Array Camera onboard the *Spitzer Space Telescope* (see Table 1).

ID	RA_HMS	DEC_DMS	EXPTIME	DATE_OBS	DS_IDENT
1	17h06m11.6s	+73d40m11s	0.4	2003-10-08T11:55:51.356	ads/sa.spitzer#0006875392
2	17h06m11.1s	+73d40m11s	0.4	2003-10-08T12:08:56.748	ads/sa.spitzer#0006876672
3	17h06m10.8s	+73d40m10s	0.4	2003-10-08T12:22:01.538	ads/sa.spitzer#0006876928
4	17h06m10.6s	+73d40m09s	0.4	2003-10-08T12:35:06.524	ads/sa.spitzer#0006877184
5	17h06m11.3s	+73d40m12s	0.4	2003-10-08T12:48:11.510	ads/sa.spitzer#0006877440
6	17h06m10.9s	+73d40m12s	0.4	2003-10-08T13:01:16.496	ads/sa.spitzer#0006877696
7	17h06m10.5s	+73d40m11s	0.4	2003-10-08T13:14:21.489	ads/sa.spitzer#0006877952
8	17h06m10.2s	+73d40m11s	0.4	2003-10-08T13:27:26.471	ads/sa.spitzer#0006878208
9	17h06m11.0s	+73d40m14s	0.4	2003-10-08T13:40:31.472	ads/sa.spitzer#0006878464
10	17h06m10.7s	+73d40m13s	0.4	2003-10-08T13:53:36.446	ads/sa.spitzer#0006878720
11	17h06m10.5s	+73d40m13s	0.4	2003-10-08T14:06:41.436	ads/sa.spitzer#0006878976
12	17h06m10.0s	+73d40m12s	0.4	2003-10-08T14:19:46.422	ads/sa.spitzer#0006879232
13	17h06m11.0s	+73d40m15s	0.4	2003-10-08T14:32:51.423	ads/sa.spitzer#0006879488
14	17h06m10.5s	+73d40m15s	0.4	2003-10-08T15:06:39.788	ads/sa.spitzer#0006879744
15	17h06m10.3s	+73d40m14s	0.4	2003-10-08T15:19:44.785	ads/sa.spitzer#0006880000
16	17h06m10.0s	+73d40m13s	0.4	2003-10-08T15:32:49.763	ads/sa.spitzer#0006880256

Table 1. IRAC Ch1 Observations of PPM 9412.

The IRAC basic calibrated data (BCD) images were retrieved from the Spitzer data archive. These observations were analyzed with the imexamine task of NOAO's Image Reduction and Analysis Facility (IRAF; [3–4]) package and a new experimental version of the MATPHOT [5] photometric reduction package, called MPDZ, which uses the following relative intrapixel quantum efficiency (QE) variation map [6] for IRAC Channel 1 (Ch1),

$$\text{intrapix} = \begin{pmatrix} 0.813 & 0.875 & 0.875 & 0.875 & 0.813 \\ 0.875 & 1.000 & 1.000 & 1.000 & 0.875 \\ 0.875 & 1.000 & 1.000 & 1.000 & 0.875 \\ 0.875 & 1.000 & 1.000 & 1.000 & 0.875 \\ 0.813 & 0.875 & 0.875 & 0.875 & 0.813 \end{pmatrix},$$

and a theoretical IRAC Ch1 PSF [7] for the central region of IRAC Ch1 (see Fig. 2).

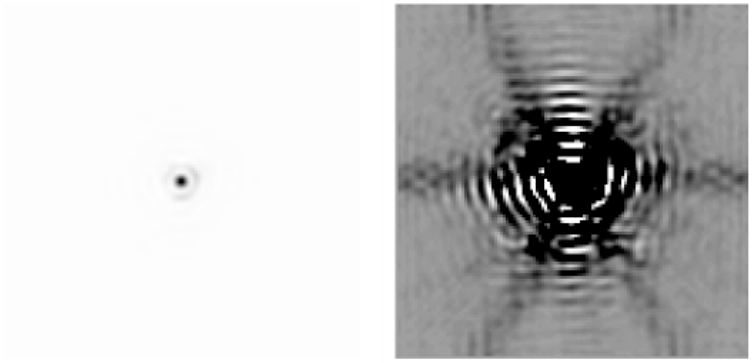

Fig. 2. A theoretical 5x5 supersampled version of the IRAC PSF for the central region of Ch1 [7]. The left side of 4 shows a linear stretch of the PSF and the right side shows a log stretch. Although the PSF appears to be reasonable in the linear stretch, which emphasizes the bright central core, the log stretch shows the numerous weak higher-spatial-frequency features of this very complicated PSF. IRAC Ch1 PSFs are significantly undersampled by the IRAC Ch1 camera [2].

3. SQUARE APERTURE PHOTOMETRY

Square aperture photometry with a 21x21 pixel box centered on the star was done using the interactive "m" keyboard command of IRAF's **imexamine** task. Fig. 3 shows a 5.6% peak-to-peak spread in these square aperture flux measurements.

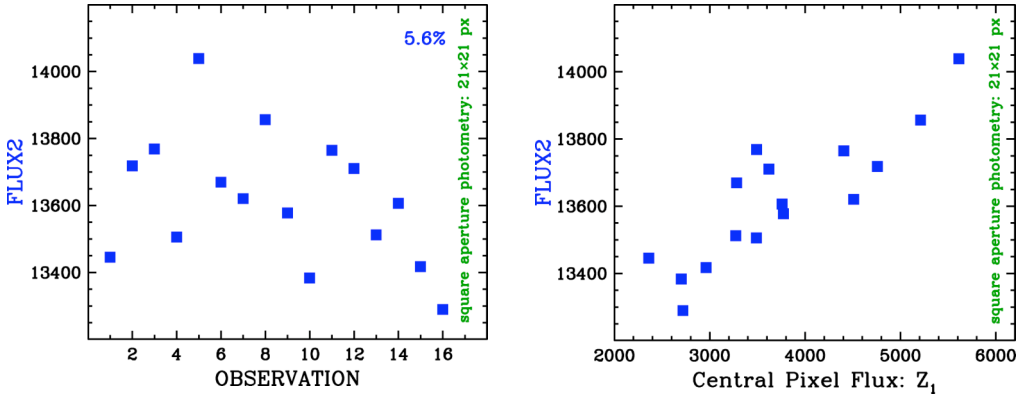

Fig. 3. Square aperture photometry (21x21 pixels)

The variation in flux seen in Fig. 3 is not completely random. The right graph of Fig. 3 shows that the total stellar flux is correlated with the amount of flux found in the central pixel. Examination of the individual observations

reveal that the observations with the most stellar flux have stellar images that are centered in the middle of a pixel while those observations with the least stellar flux are centered on a pixel corner. This same effect is seen in Fig. 4 which is taken from the IRAC Data Handbook [8].

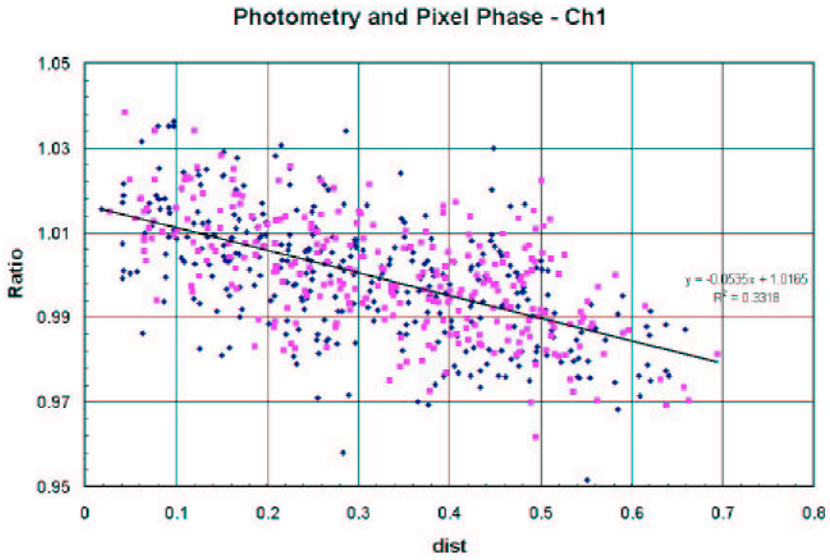

Fig. 4. Normalized measured flux density (y-axis) is plotted against the distance of the source centroid from the center of a pixel (source: Fig. 5.1 of the IRAC Data Handbook [8]).

The flux density of a point source measured from IRAC images depends on the exact location where the peak of the stellar image (the Point Response Function) falls within the central pixel of the stellar image. This effect is due to the variations in the quantum efficiency of a pixel, and combined with the undersampling of the PRF, it is most severe in Channel 1 [8]. The correction can be as much as 4% peak to peak.

4. CIRCULAR APERTURE PHOTOMETRY

Circular aperture photometry centered on the star with a radius of 10 pixels was done using the interactive "a" keyboard command of IRAF's imexamine task. Fig. 5 shows a 4.5% peak-to-peak spread in the raw circular aperture flux measurements (open circles) with a radius of 5 pixels. Applying the recommended Ch1 flux correction from the IRAC Data Handbook reduces the peak-to-peak spread to 3.5% (filled circles).

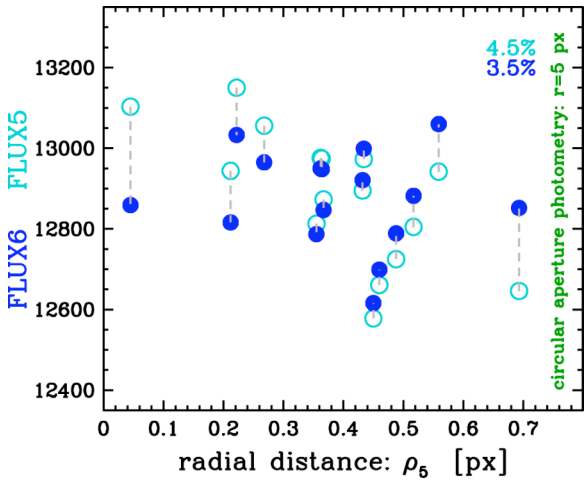

Fig. 5. Circular aperture photometry (radius of 5 pixels)

5. MATPHOT SIMULATIONS: PART I

Ten thousand IRAC Ch1 observations of a single star on a flat background were simulated and analyzed with MPDZ. Each stellar observation was simulated using the theoretical 5x5 supersampled IRAC Ch1 PSF shown in Fig. 2; a star with 10^6 electrons was located near the center of an field of 60x60 pixels on a flat background of 100 electrons. The horizontal axis of the left graph of Fig. 6 shows the subpixel offset (distance) the center of a star is from the middle of a pixel; stars centered near the middle of a pixel will have small offset values while stars located near the corner of a pixel will have offsets near 0.7 px. The vertical axis of the left graph of Fig. 6 shows the absolute flux ratio of the total fluxes divided by the true flux of 10^6 electrons. The cyan points show the *observed* absolute flux ratios and the blue points show the measured absolute flux ratios as reported by MPDZ. Note that while the *average* stellar observation suffered an absolute flux loss of about 9%, stars centered near the middle of a pixel suffered, on average, an absolute flux loss of about 7% as compared to an absolute flux loss of about 11% for stars centered near a pixel corner. It is important to note that *the vertical scatter seen in the observed flux ratios is not random but systematic*; a simple radial correction function can only partially recover the lost flux. The *measured* absolute flux ratios are clustered around unity and are not a function of subpixel offset; the vertical scatter seen in the measured absolute flux ratios is random. By modeling the image formation process within the detector, MPDZ was able to able fully recover all of the stellar flux lost due to the non-uniform IRAC Ch1 intrapixel quantum efficiency variations.

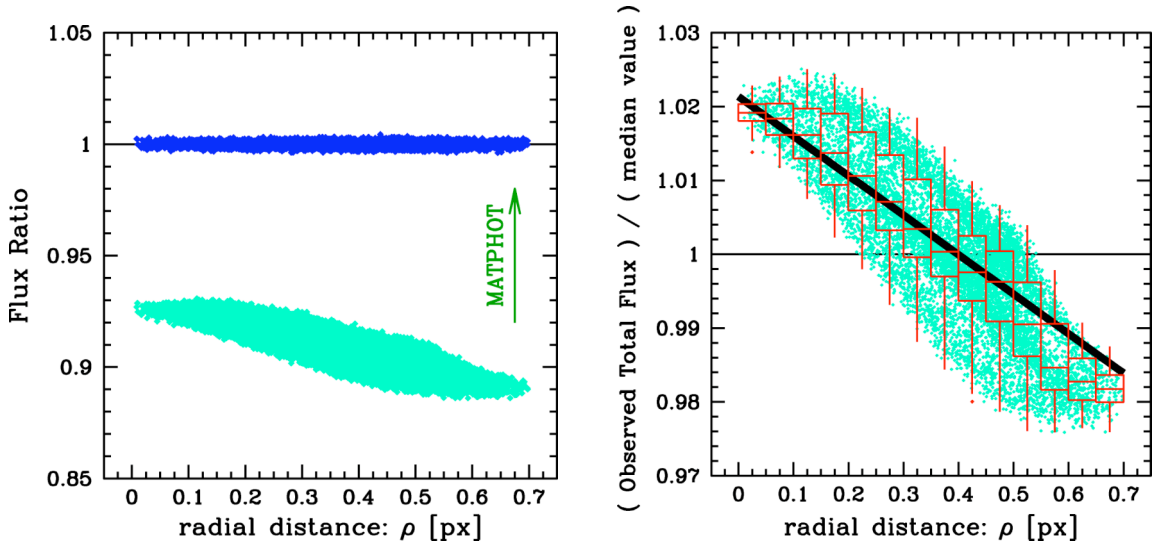

Fig. 6. Results of the MPDZ experiment with simulated IRAC Ch1

The vertical axis of the right graph of Fig. 6 shows the *observed* (apparent) total flux divided by the *median observed* total flux value of all ten thousand stars. The median values of the box-and-whisker plots (the central horizontal bar in each box) range from an excess flux of about 2% for stars centered near the center of a pixel to a flux deficit of about 2% for stars centered near the corner of a pixel. Note that this graph reproduces almost exactly the observed flux loss distribution seen in Fig. 5.1 of the IRAC Data Handbook [8]. One sees that even after the recommended flux correction (thick line of right graph of Fig. 6) is applied an approximate peak-to-peak spread of about 3% would remain for many observations – and that is exactly what is seen in Fig. 5.

6. MATPHOT PHOTOMETRY

MATPHOT PSF-fitting photometry was performed on all of the observations using MPDZ with the theoretical 5x5 supersampled IRAC Ch1 PSF shown in Fig. 2. The open diamonds in Fig. 7 show a 5.2% peak-to-peak spread in the raw measured stellar flux values reported by MPDZ.

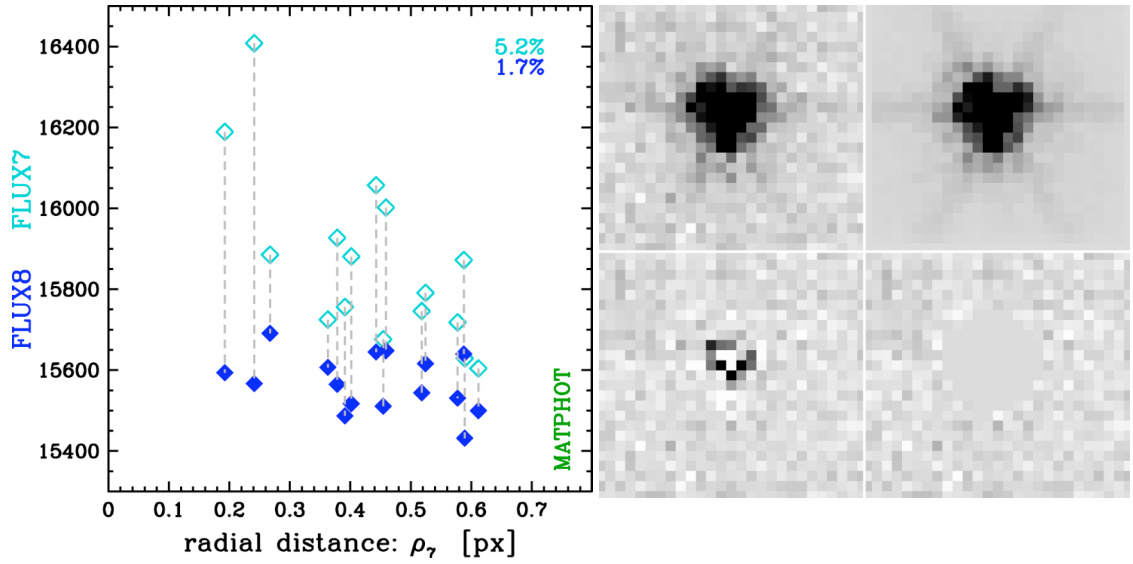

Fig. 7. MATPHOT (MPDZ) photometry

The upper-left image in Fig. 7 shows central portion of the first IRAC Ch1 observation in Table 1. The noiseless best-fit model of the observation is shown in the upper-right image. The residuals remaining after the best-fit model is subtracted from the observation are shown in the lower-left image. The lower-right image is the same as the residual image except that all residuals within a radius of 5 pixels from the fitted center of the star have been set to zero. All of these images are displayed with the same negative linear stretch which was chosen to emphasize the faint features of the stellar image.

The filled diamonds in Fig. 7 show a 1.7% peak-to-peak spread; these flux values are the combination of the raw measured stellar fluxes (open diamonds) with the sum of all of residuals (positive and negative) within a radius of 5 pixels from the fitted center of the star.

MATPHOT with residuals yield an improvement in photometric precision of more than 100% over the best results obtained with aperture photometry. The left graph of Fig. 8 compares MATPHOT photometry with residuals (FLUX8: filled diamonds in Fig. 7) with the best corrected circular photometry (FLUX6: filled circles in Fig. 5). The errorbars plotted with the FLUX8 values are the errors estimated by MPDZ for the raw MATPHOT flux estimates (FLUX7: open diamonds in Fig. 7).

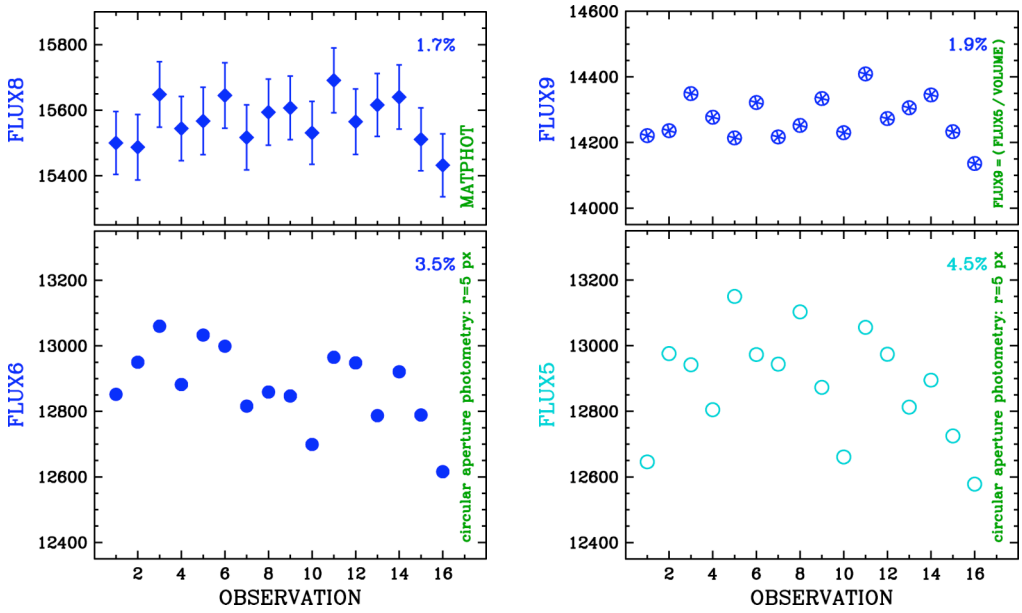

Fig. 8. Comparison between MATPHOT and aperture photometry

We see that although the recorded flux of point sources was corrupted by using lossy detectors with large intrapixel quantum efficiency variations, it is possible to significantly improve the precision of stellar photometry from observations made with such detectors – if the image formation process inside the detector is accurately modeled.

Simple aperture photometry of stellar observations obtained with IRAC Ch1 can be significantly improved by simply dividing the measured aperture flux with the volume of the Point Response Function (PRF) which is the convolution of the Point Spread Function and the discrete Detector Response Function. The right graph of Fig. 8 compares the best uncorrected circular photometry (FLUX5: open circles in Fig. 5) with those flux values divided by the volume of the best-fit PRF computed by MPDZ. The resultant peak-to-peak spread is 1.9% which is just slightly worse than the 1.7% spread from the MATPHOT with residual results. This suggests that aperture photometry from IRAC Ch1 observations could probably be significantly improved by using a two-dimensional correction function instead of using the radial correction function currently recommended in the IRAC Data Handbook. The derivation of that two-dimensional correction function would require a detailed analysis of a large number of dithered IRAC Ch1 unsaturated stellar observations.

7. MATPHOT SIMULATIONS: PART II

I determined a new two-dimensional flux correction based on the computed MATPHOT Point Response Function (PRF) volumes of 100,000 artificial stellar observations. Median values were determined on a 11x11 grid of the central pixel of the PRF. Columns 1 and 2 of Table 2 give, respectively, the pixel offset from the center of the pixel in the *x* and *y* directions in pixel units; the third column gives the radial distance from the center of the pixel in pixel units. Columns 5 and 6 give the respective subpixel offset in the *x* and *y* directions; the values range from -5 to 5 with the central subpixel having idx and idy values of zero. Column 6 gives the new flux correction which can be compared with the value given in last column (idhcorr) which is the recommended flux correction given in the IRAC Data Handbook .

Table 2. New IRAC Ch1 Aperture Correction (column 6).

# dx	dy	dr	idx	idy	newcorr	idhcorr
-0.4545	-0.4545	0.6428	-5	-5	0.9822	0.9870
-0.3636	-0.4545	0.5821	-4	-5	0.9823	0.9902
-0.2727	-0.4545	0.5301	-3	-5	0.9856	0.9930
-0.1818	-0.4545	0.4896	-2	-5	0.9909	0.9952
-0.0909	-0.4545	0.4635	-1	-5	0.9962	0.9965
0.0000	-0.4545	0.4545	0	-5	1.0005	0.9970
0.0909	-0.4545	0.4635	1	-5	1.0019	0.9965
0.1818	-0.4545	0.4896	2	-5	1.0005	0.9952
0.2727	-0.4545	0.5301	3	-5	0.9962	0.9930
0.3636	-0.4545	0.5821	4	-5	0.9905	0.9902
0.4545	-0.4545	0.6428	5	-5	0.9851	0.9870
-0.4545	-0.3636	0.5821	-5	-4	0.9877	0.9902
-0.3636	-0.3636	0.5143	-4	-4	0.9877	0.9938
-0.2727	-0.3636	0.4545	-3	-4	0.9912	0.9970
-0.1818	-0.3636	0.4066	-2	-4	0.9962	0.9996
-0.0909	-0.3636	0.3748	-1	-4	1.0019	1.0013
0.0000	-0.3636	0.3636	0	-4	1.0060	1.0019
0.0909	-0.3636	0.3748	1	-4	1.0074	1.0013
0.1818	-0.3636	0.4066	2	-4	1.0060	0.9996
0.2727	-0.3636	0.4545	3	-4	1.0017	0.9970
0.3636	-0.3636	0.5143	4	-4	0.9957	0.9938
0.4545	-0.3636	0.5821	5	-4	0.9903	0.9902
-0.4545	-0.2727	0.5301	-5	-3	0.9937	0.9930
-0.3636	-0.2727	0.4545	-4	-3	0.9939	0.9970
-0.2727	-0.2727	0.3857	-3	-3	0.9972	1.0007
-0.1818	-0.2727	0.3278	-2	-3	1.0024	1.0038
-0.0909	-0.2727	0.2875	-1	-3	1.0082	1.0060
0.0000	-0.2727	0.2727	0	-3	1.0122	1.0068
0.0909	-0.2727	0.2875	1	-3	1.0140	1.0060
0.1818	-0.2727	0.3278	2	-3	1.0123	1.0038
0.2727	-0.2727	0.3857	3	-3	1.0078	1.0007
0.3636	-0.2727	0.4545	4	-3	1.0018	0.9970
0.4545	-0.2727	0.5301	5	-3	0.9964	0.9930
-0.4545	-0.1818	0.4896	-5	-2	0.9988	0.9952
-0.3636	-0.1818	0.4066	-4	-2	0.9990	0.9996
-0.2727	-0.1818	0.3278	-3	-2	1.0023	1.0038
-0.1818	-0.1818	0.2571	-2	-2	1.0077	1.0076
-0.0909	-0.1818	0.2033	-1	-2	1.0133	1.0105
0.0000	-0.1818	0.1818	0	-2	1.0176	1.0116
0.0909	-0.1818	0.2033	1	-2	1.0192	1.0105
0.1818	-0.1818	0.2571	2	-2	1.0175	1.0076
0.2727	-0.1818	0.3278	3	-2	1.0130	1.0038
0.3636	-0.1818	0.4066	4	-2	1.0074	0.9996
0.4545	-0.1818	0.4896	5	-2	1.0017	0.9952
-0.4545	-0.0909	0.4635	-5	-1	1.0011	0.9965
-0.3636	-0.0909	0.3748	-4	-1	1.0014	1.0013
-0.2727	-0.0909	0.2875	-3	-1	1.0047	1.0060
-0.1818	-0.0909	0.2033	-2	-1	1.0101	1.0105
-0.0909	-0.0909	0.1286	-1	-1	1.0158	1.0145
0.0000	-0.0909	0.0909	0	-1	1.0200	1.0165
0.0909	-0.0909	0.1286	1	-1	1.0216	1.0145
0.1818	-0.0909	0.2033	2	-1	1.0201	1.0105
0.2727	-0.0909	0.2875	3	-1	1.0154	1.0060
0.3636	-0.0909	0.3748	4	-1	1.0095	1.0013
0.4545	-0.0909	0.4635	5	-1	1.0039	0.9965
-0.4545	0.0000	0.4545	-5	0	1.0004	0.9970
-0.3636	0.0000	0.3636	-4	0	1.0006	1.0019

-0.2727	0.0000	0.2727	-3	0	1.0036	1.0068
-0.1818	0.0000	0.1818	-2	0	1.0088	1.0116
-0.0909	0.0000	0.0909	-1	0	1.0147	1.0165
0.0000	0.0000	0.0000	0	0	1.0188	1.0213
0.0909	0.0000	0.0909	1	0	1.0206	1.0165
0.1818	0.0000	0.1818	2	0	1.0188	1.0116
0.2727	0.0000	0.2727	3	0	1.0145	1.0068
0.3636	0.0000	0.3636	4	0	1.0086	1.0019
0.4545	0.0000	0.4545	5	0	1.0031	0.9970
-0.4545	0.0909	0.4635	-5	1	0.9963	0.9965
-0.3636	0.0909	0.3748	-4	1	0.9963	1.0013
-0.2727	0.0909	0.2875	-3	1	0.9994	1.0060
-0.1818	0.0909	0.2033	-2	1	1.0047	1.0105
-0.0909	0.0909	0.1286	-1	1	1.0103	1.0145
0.0000	0.0909	0.0909	0	1	1.0146	1.0165
0.0909	0.0909	0.1286	1	1	1.0161	1.0145
0.1818	0.0909	0.2033	2	1	1.0145	1.0105
0.2727	0.0909	0.2875	3	1	1.0101	1.0060
0.3636	0.0909	0.3748	4	1	1.0044	1.0013
0.4545	0.0909	0.4635	5	1	0.9988	0.9965
-0.4545	0.1818	0.4896	-5	2	0.9901	0.9952
-0.3636	0.1818	0.4066	-4	2	0.9902	0.9996
-0.2727	0.1818	0.3278	-3	2	0.9933	1.0038
-0.1818	0.1818	0.2571	-2	2	0.9983	1.0076
-0.0909	0.1818	0.2033	-1	2	1.0040	1.0105
0.0000	0.1818	0.1818	0	2	1.0078	1.0116
0.0909	0.1818	0.2033	1	2	1.0099	1.0105
0.1818	0.1818	0.2571	2	2	1.0082	1.0076
0.2727	0.1818	0.3278	3	2	1.0037	1.0038
0.3636	0.1818	0.4066	4	2	0.9981	0.9996
0.4545	0.1818	0.4896	5	2	0.9928	0.9952
-0.4545	0.2727	0.5301	-5	3	0.9838	0.9930
-0.3636	0.2727	0.4545	-4	3	0.9839	0.9970
-0.2727	0.2727	0.3857	-3	3	0.9873	1.0007
-0.1818	0.2727	0.3278	-2	3	0.9922	1.0038
-0.0909	0.2727	0.2875	-1	3	0.9976	1.0060
0.0000	0.2727	0.2727	0	3	1.0016	1.0068
0.0909	0.2727	0.2875	1	3	1.0036	1.0060
0.1818	0.2727	0.3278	2	3	1.0019	1.0038
0.2727	0.2727	0.3857	3	3	0.9977	1.0007
0.3636	0.2727	0.4545	4	3	0.9920	0.9970
0.4545	0.2727	0.5301	5	3	0.9866	0.9930
-0.4545	0.3636	0.5821	-5	4	0.9798	0.9902
-0.3636	0.3636	0.5143	-4	4	0.9798	0.9938
-0.2727	0.3636	0.4545	-3	4	0.9830	0.9970
-0.1818	0.3636	0.4066	-2	4	0.9881	0.9996
-0.0909	0.3636	0.3748	-1	4	0.9936	1.0013
0.0000	0.3636	0.3636	0	4	0.9978	1.0019
0.0909	0.3636	0.3748	1	4	0.9991	1.0013
0.1818	0.3636	0.4066	2	4	0.9978	0.9996
0.2727	0.3636	0.4545	3	4	0.9937	0.9970
0.3636	0.3636	0.5143	4	4	0.9879	0.9938
0.4545	0.3636	0.5821	5	4	0.9824	0.9902
-0.4545	0.4545	0.6428	-5	5	0.9787	0.9870
-0.3636	0.4545	0.5821	-4	5	0.9787	0.9902
-0.2727	0.4545	0.5301	-3	5	0.9818	0.9930
-0.1818	0.4545	0.4896	-2	5	0.9873	0.9952
-0.0909	0.4545	0.4635	-1	5	0.9927	0.9965
0.0000	0.4545	0.4545	0	5	0.9969	0.9970
0.0909	0.4545	0.4635	1	5	0.9982	0.9965

0.1818	0.4545	0.4896	2	5	0.9969	0.9952
0.2727	0.4545	0.5301	3	5	0.9925	0.9930
0.3636	0.4545	0.5821	4	5	0.9868	0.9902
0.4545	0.4545	0.6428	5	5	0.9814	0.9870

Fig. 9 shows the new two-dimensional correction (*121 blue points*) with respect to the the standard radial correction (*black line*) for the new 100,000 simulated observations. Note how much better the new flux correction samples the "cloud" of relative flux loss measurements than the standard flux correction recommended by the IRAC Data Handbook.

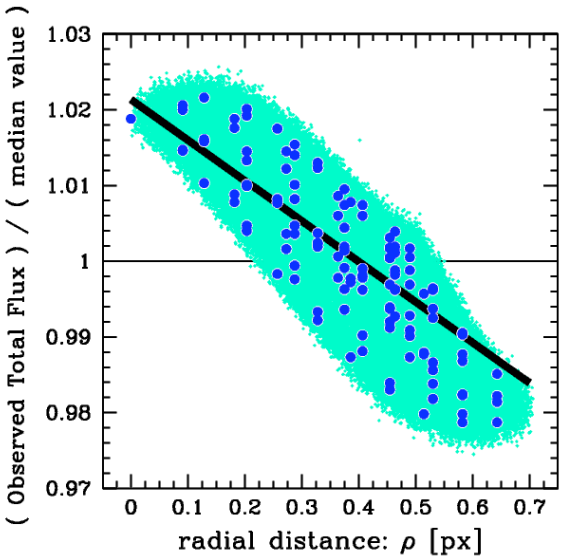

Fig. 9. Comparison of the new flux correction (121 blue points) with the radial correction (black line) in the IRAC Data Handbook.

8. APPLICATION OF THE NEW FLUX CORRECTION

Fig. 10 is a new version of Fig. 5 with the red points showing the application of the new flux correction based on centroid positions determined from aperture photometry. I expected to see a peak-to-peak variation of about 2% but the measured variation was 3%. So what went wrong?

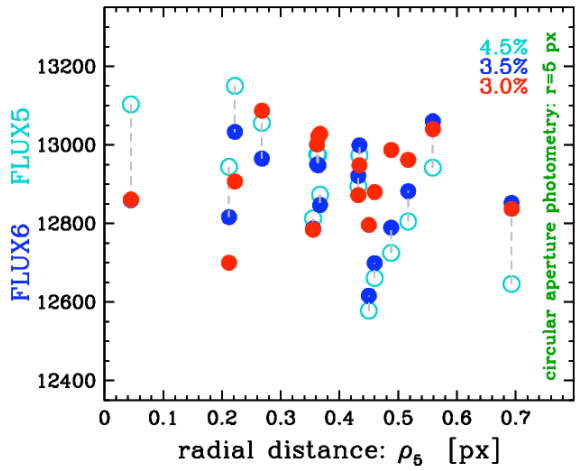

Fig. 10. Circular aperture photometry (radius of 5 pixels) with the new flux correction (red filled circles) *based on positions from aperture photometry*

Fig. 11 shows that systematic correction errors of 1% are not uncommon because the *wrong position* (from aperture photometry*) was used*! The ***measured position***, based on the intensity-weighted mean centroid, can be ***systematically off*** by as much as ***one-sixth of a pixel*** (0.2 arcsec) from the ***true position*** due to nonuniform intrapixel quantum efficiency variation. Note that the peak of the new flux correction is ***not*** in the center of the central pixel; this is probably due to the convolution of the asymmetric IRAC PSF (due mainly to trefoil aberration) with the nonuniform intrapixel quantum efficiency map.

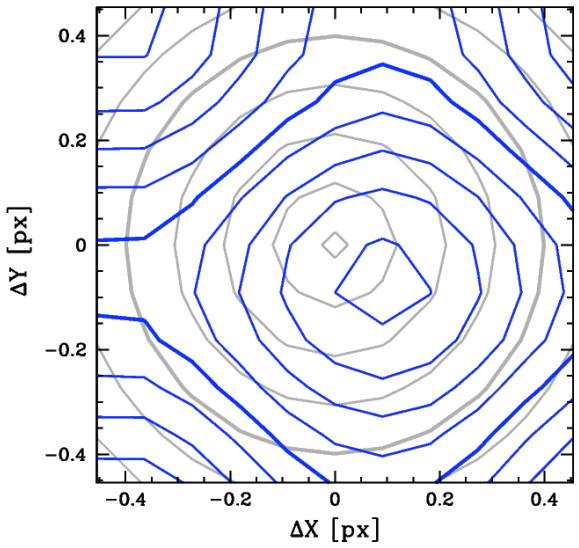

Fig. 11. Comparision of the new flux corrction (blue contours) with the flux correction from the IRAC Data Handook (gray contours). The contours of the standard correction range from 0.99 to 1.02 in steps of 0.005 (0.5%); the contours of the new correction range from 0.98 to 1.02 in steps of 0.005.

Better positions should give better corrections. So… make better centroid measurements using knowledge about the nonuniform intrapixel quantum efficiency variation – say, for example, as determined using MATPHOT. Fig. 12 is a new version of Fig. 10 with the orange diamonds showing the application of the new flux correction based on centroid positions determined from MAPHOT photometry. *The measured peak-to-peak variation is 1.7% which matches the variations found using MATPHOT photometry with residuals.*

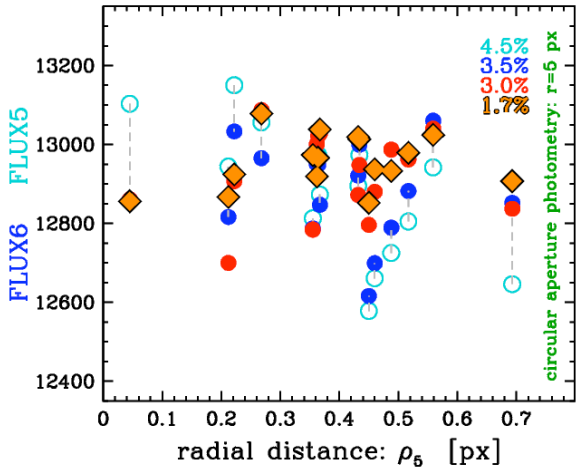

Fig. 12. Circular aperture photometry (radius of 5 pixels) with the new flux correction (red filled circles) *based on positions from MATPHOT photometry*.

The new two-dimensional flux correction yields an improvement of 100% over the standard correction given in the IRAC Data Handbook when given accurate centroid estimates.

9. SUMMARY AND DISCUSSION

This detailed analysis of multiple observations of a single bright isolated star obtained with Channel 1 of the *Spitzer Space Telescope*'s Infrared Array Camera (IRAC) instrument yields an improvement in photometric precision of more than 100% over the best results obtained with aperture photometry. The improvement is achieved by accurately modeling the image formation process within lossy detectors that exhibit large intrapixel quantum efficiency variations.

Mitigating the impact of flux loss problems seen in state-of-the-art NASA-grade infrared detectors is still in its early days. Hoffmann's IRAC Ch1 intrapixel QE map is the *first attempt* by the IRAC team to quantify this effect. Derivation of the intrapixel QE map is an *iterative process* due to the apparent centroid shifting caused by the non-uniform QE variation across a pixel; given an initial estimate of the intrapixel QE map, better positions of the input stellar images can then be determined, which, in turn, enables a better measurement of the intrapixel QE map to be made

Much more work remains to be done. However, the possibility of significantly improving the precision and accuracy of space-based near-infrared stellar photometry and astrometry appears to be excellent.

Work has recently begun with the IRAC Instrument Team on a *SST* Cycle 4 archival grant (*Improving the Photometric Precision of IRAC Channels 1 and 2*) which will investigate the development of new calibration procedures for IRAC Ch1 and Ch2 that have the potential of significantly improving the precision of IRAC point-source photometry. This timely research effort is intended to not only enhance the science return of existing IRAC Ch1 and Ch2 observations in the Spitzer Data Archive but also those that will be made in the future during the Spitzer Warm Mission.

I wish to thank Bill Glaccum, Bill Hoffmann, David Elliott, Patrick Lowrance, and the rest of the IRAC team for their support of this research effort. This work has been supported by a grant from the National Aeronautics and Space Administration (NASA), Interagency Order No. NNG06EC81I, which was awarded by the Applied Information Systems Research (AISR) Program of NASA's Science Mission Directorate.

10. REFERENCES

1. Gehrz, R. D., The NASA Spitzer Space Telescope, Review of Scientific Instruments, Vol. 78, 011302:1-38, 2007.
2. Fazio, G. G., et al., The Infrared Array Camera (IRAC) for the Spitzer Space Telescope, ApJS, Vol. 154, 10-17, 2004.
3. Tody, D., The *IRAF* Data Reduction and Analysis System, *Instrumentation in Astronomy VI,* Proceedings of the SPIE, Vol. 627, 733, 1986.
4. Tody, D., IRAF in the Nineties, *Astronomical Data Analysis Software and Systems II,* ASP Conf. Ser. 52, 173, 1993.
5. Mighell, K. J., Stellar photometry and astrometry with discrete point spread functions, MNRAS, Vol. 361, 861-878, 2005.
6. Hoffmann, B., Intra-pixel Variation Effect on Aperture Photometry, IRAC/TMo5-028 (Simfit Report 59; Version 2: December 10, 2005), 2005.
7. Hoffmann, B., 25 Position Model Pixel Repsonse Functions (PRF) Description and Quality, IRAC/TMo5-014 Simfit Report 52; September 3, 2005), 2005.
8. Reach, W. T., et al., Infrared Array Camera Data Handbook (Version 3.0; January 20, 2006), 2006.